I&EC research
Industrial & Engineering Chemistry Research

pubs.acs.org/IECR

Article

Electrochemical Aging and Halogen Oxides Formation on Multiwalled Carbon Nanotubes and Fe_3O_4@g-C_3N_4 Coated Conductive Membranes

Qingquan Ma, Jianan Gao, Courtney Potts, Xiao Tong, Yi Tao, and Wen Zhang*

Cite This: *Ind. Eng. Chem. Res.* 2022, 61, 14260−14271

Read Online

ACCESS | Metrics & More | Article Recommendations | Supporting Information

ABSTRACT: Electrochemical membrane filtration is widely reported to enhance water contaminants' degradation or rejection via anodic oxidation or cathodic repulsion. Despite their advances, electrochemical membranes or electrocatalysts often suffer from corrosion or passivation, especially under strong electrode potentials or reactions. Moreover, the formation of toxic byproducts, such as chlorinated organic compounds and oxyhalides (e.g., ClO_4^-) is another major concern. This study investigated the membrane aging processes of two types of conductive membranes, multiwalled carbon nanotubes (MWCNTs) and ferrite/graphitic carbon nitride hybrids (Fe_3O_4@g-C_3N_4) coated on ceramic membranes. Under high current densities (~20 mA·cm^{-2}) with anodic potentials (~10 V), MWCNTs and Fe_3O_4@g-C_3N_4 catalysts underwent evident oxidation as indicated by an increase of the intensity ratio of the Raman spectral bands (I_D/I_G) and charge transfer resistance (R_{ct}) of two electrochemical membranes. Under variations of electrode potentials, chloride or bromide were shown to be oxidized to bromate (BrO_3^-) and chlorate (ClO_3^-) at levels of 1−10 mmol·L^{-1}. The formation of BrO_3^- and ClO_3^- was dependent on the solution pH, current densities (1−20 mA·cm^{-2}), and initial concentrations of Br or Cl ions. To warrant a safe and rational design and operation of electrochemically reactive membrane processes, membrane aging and toxic byproduct's formation deserve careful characterization under relevant water filtration environments.

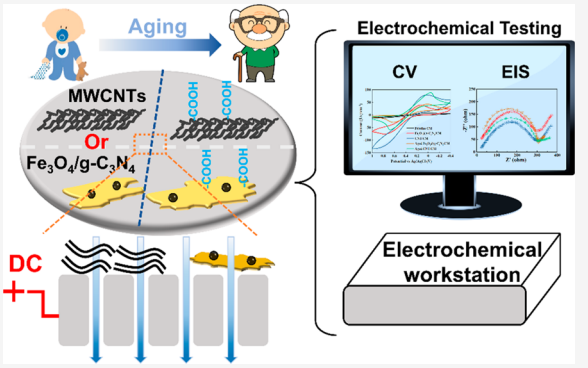

1. INTRODUCTION

Electrically charged or electrochemically reactive membranes (ERMs) integrate electrochemical advanced oxidation and/or electrochemical reduction reactions into membrane filtration to enhance pollutant degradation, rejection, or transformation (e.g., nitrification).[1,2] Electrochemical membrane filtration has demonstrated promising concurrent rejection and degradation of diverse contaminants for water purification and wastewater treatment.[3] For example, effective removal of persistent organic pollutants (e.g., polycyclic aromatic hydrocarbons and polychlorinated biphenyls), dyes, pharmaceutical residuals, and personal care products, and perfluorochemicals as well as microbial species were reported.[4−8] In a typical configuration, the constituents of influent serve as the electrolyte, and ERMs act in the dual function of separation unit and electrode. Such a design can improve electrochemical kinetics and efficiencies by the increased electro-active surface area and the enhanced convective mass transfer of pollutants.[9,10] When the proper electrode potentials (e.g., 1−2 V) are applied to ERMs, anodic or cathodic reactions may take place and generate diffusive radicals or reactive species such as reactive oxygen/chlorine species, causing direct or indirect oxidation or reduction of the aqueous species.[11,12]

Electrochemical membranes are featured for high electrical conductivity, electrochemical activity, and water permeability. Various organic and inorganic materials have been reported to fabricate ERMs, including conductive polymers (e.g., polyaniline, polythiophene, and polyacetylene),[13,14] carbon-based nanomaterials such as multiwall carbon nanotubes (MWCNTs) and graphite,[15,16] metallic membranes (e.g., Cu),[17] and ceramic/metal oxides membranes such as alumina (Al_2O_3), zirconia (ZrO_2), and titania (TiO_2)), silica (SiO_2), and Magnéli phase Ti_4O_7).[2,18] Conductive ceramic membranes particularly demonstrate high chemical inertness, excellent thermal stability, outstanding mechanical strength, and long service life. Except for the Magnéli phase Ti_4O_7, most ceramic materials (e.g., Al_2O_3, ZrO_2, and TiO_2) are nonconductive and require the construction of a conductive catalyst layer for electrochemical reactions. For example, MWCNTs-based

Received: August 9, 2022
Revised: September 1, 2022
Accepted: September 6, 2022
Published: September 15, 2022

https://doi.org/10.1021/acs.iecr.2c02847
Ind. Eng. Chem. Res. 2022, 61, 14260−14271

materials and carbon−metal nanohybrids (e.g., Fe_3O_4 conjugated with g-C_3N_4) as a conductive layer were reported due to their high conductivity and reactivity.[19,20] Zhang et al. coated CNTs onto a ceramic membrane by pyrolysis for organic wastewater treatment.[21] Wang et al. reported that CNT-functionalized ceramic membrane possessed high hydrophilicity, permeability, and conductivity, which promoted the generation of reactive (radical) chlorine species (RCS) through the anodization of chloride ions for membrane self-cleaning.[22]

Practical implementations of electrochemical membranes are largely hampered by electrode material stability and operational cost for long-term use.[23] For instance, ERMs are often needed to operate at relatively high overpotentials to effectively degrade persistent pollutants. However, high electrode potentials cause high electrical consumption and risks of inducing undesirable water oxidation or oxygen evolution on anode or chlorine or hydrogen gas evolution on cathode.[5] Furthermore, high electrode potentials may lead to detrimental impacts on electrochemical membrane properties (e.g., aging or passivation), as characterized by the loss of conductivity, reactivity, and even mechanical integrity or stability.[24] However, only a few studies have reported the membrane aging on limited materials such as the Magnéli phase Ti_4O_7 that could be oxidized into TiO_2 or other titanium phases in oxidative environments.[2] Halali et al. also reported that CNT/PVA-coated electrically conductive membranes were physically unstable during the filtration as indicated by the PVA leaching under 2−4 V vs Ag/AgCl reference electrode.[25] Three standardized methods such as electrochemical oxidation, surface scratch testing, and pressurized leaching were employed to assess the electrochemical, chemical, and physical stability of such membrane coatings.[26] The related aging mechanisms are not well understood and deserve research efforts to support the rational design and operation of electrochemical membrane systems.

The other important concern is the formation of poisonous halo-oxyanions and halogenated byproducts in the electrochemical treatment.[27] Strong anodic oxidation could yield chlorate (ClO_3^-), perchlorate (ClO_4^-), and bromate (BrO_3^-) in the treated water,[28] especially when Cl^- and Br^- concentrations are high (500−4000 mM). ClO_4^- is laborious to reduce to Cl^- once it is formed and presents serious health risks. The halogenation of organic compounds can lead to the production of halogenated byproducts such as trihalomethane and polybrominated biphenyl that are significantly more toxic than the precursor compounds. However, electrochemical production of these halogen oxides or halogenated organic matters requires certain reaction times due to relatively low reaction rate constants (e.g., the formation rate constant of ClO_3^- is around $(2.4-12) \times 10^{-6}$ s^{-1}).[29] To avoid these byproducts and address this critical challenge, applying proper electrode potentials is essential.

The objectives of this study aim to unravel electrochemical membrane aging mechanisms and byproducts formation using two model electrocatalyst-membranes: hybridized MWCNTs coated ceramic membrane (MWCNTs/CM) and Fe_3O_4@g-C_3N_4 loaded ceramic membrane (Fe_3O_4@g-C_3N_4/CM), which have been reported for the degradation of organic dyes,[30] tetrabromobisphenol A (TBBPA),[31] and diclofenac.[32] For example, g-C_3N_4 hybrids with Fe_3O_4 composite have been reported with better electrochemical performance than pure g-C_3N_4.[33,34] Membrane filtration experiments were performed in the single pass, permeate flow-through operational mode under variations of the initial concentrations of sodium chloride (NaCl) and sodium bromide (NaBr), solution pH, and applied electrode potentials. The membrane aging of the two types of hybridized ERMs were thoroughly characterized by examining the changes of the membrane's physicochemical and electrochemical properties. Halogenated byproducts in the filtrate were analyzed to establish connections with operational factors such as applied current densities and solution pH values. Ultimately, this work promotes the durable design and operations of efficient and safe electrochemical membrane water filtration.

2. MATERIALS AND METHODS

2.1. Anode Membrane Preparation and Characterization. *2.1.1. Preparation of MWCNTs and MWCNTs-Coated Membrane (MWCNTs/CM).* MWCNTs (>99%) were purchased from Fisher Scientific (USA). The outer diameter and length of CNTs are 20−40 nm and 5−15 μm, respectively. To introduce oxygen-containing functional groups, which could interfere with the electron transport in the sp^2 carbonaceous structure, we prepared two kinds of MWCNTs, pristine or untreated MWCNTs (*p*-MWCNTs) and oxidized MWCNTs (*o*-MWCNTs). *p*-MWCNTs were produced by hydrochloric acid treatment of the MWCNTs. Briefly, 0.2 g of the MWCNTs powder was dispersed in 200 mL of HCl (36%) and heated at 70 °C under refluxing for 12 h. After heating, the solid sample was cooled to room temperature, rinsed by DI water, and vacuum-filtered to collect the *p*-MWCNTs. *o*-MWCNTs were prepared by the oxidation of the *p*-MWCNTs using a modified Hummers' method,[35] where 0.1 g of *p*-MWCNTs was dispersed in 60 mL of H_2SO_4 (78%) with 0.1 g of $NaNO_3$ by stirring it an ice bath for 40 min, followed by the addition of 0.2 g of $KMnO_4$ and sonication at 40 °C for 2 h. Twenty milliliters of H_2O_2 (30%) was then added, and the mixture was stirred under reflux at 70 °C for 40 min. After heating, the resulting mixture was centrifuged, diluted, vacuum-filtered, and rinsed with DI water to obtain the *o*-MWCNTs.

A commercial ceramic membrane (47N014, Sterlitech Corporation, US) was chosen as a membrane support for catalyst coating. This flat-sheet membrane is made of a zirconia/titania (Zr/TiO_2) coating on an alumina (α-Al_2O_3) owing a nominal pore size of 140 nm, a diameter of 4.6 cm, and an effective surface area of 17.34 cm^2. The membrane was rinsed rigorously with deionized (DI) water before use to remove loosely attached particles or impurities. To obtain hybridized MWCNTs-coated membrane (MWCNTs/CM), *p*-MWCNTs and *o*-MWCNTs were dispersed in DMSO at 0.5 $mg{\cdot}mL^{-1}$ with a 10:1 mass ratio followed by ultrasonication for 15 min to obtain a hybridized MWCNTs suspension, which was then vacuum filtered through the planar ceramic membrane at a loading rate of 1 $mg{\cdot}cm^{-2}$. The 10:1 mass ratio of *p*-MWCNTs and *o*-MWCNTs was chosen to obtain the optimal surface states of hydrophilicity and conductivity and high water permeability as reported previously.[22] The fabricated membrane was then rinsed by sequential filtering of 50 mL of ethanol, 50 mL of 1:1 DI water/ethanol, and 100 mL of DI water to remove the residual DMSO, followed by desiccating at 70 °C for 60 min.

2.1.2. Preparation of Fe_3O_4 NPs, Fe_3O_4 NPs@g-C_3N_4, and Fe_3O_4 NPs@g-C_3N_4-Coated Membranes. To synthesize Fe_3O_4 nanoparticles (NPs), 0.67 g of the $FeCl_3$ $6H_2O$ was dissolved

https://doi.org/10.1021/acs.iecr.2c02847
Ind. Eng. Chem. Res. 2022, 61, 14260−14271

in 50 mL of ethylene glycol to form a well-mixed solution. Then, the controlled amount of sodium acetate, (1.08 g) was added to the prepared ethylene glycol solution at room temperature under magnetic stirring. The resultant homogeneous mixture was then transferred to a 100 mL Teflon lined stainless steel autoclave and incubated at 200 °C for 24 h. After the incubation, the black solid precipitates were collected by magnetic separation and washed with ethanol three times. The final products were dried in a vacuum oven at 40 °C for 6 h. Fe_3O_4@g-C_3N_4 composites were prepared via a two-step self-assembly.[36] The g-C_3N_4 solid was prepared by heating melamine to 550 °C for 2 h in N_2 atmosphere. After that, the g-C_3N_4 solid was ground and mixed with 10 mL of methanol under ultrasonic mixing for 30 min. Finally, the mixture of Fe_3O_4 and g-C_3N_4 with a weight ratio of 5 wt % (Fe_3O_4 to g-C_3N_4) was ultrasonicated for 30 min and stirred in a fume hood for 24 h to remove methanol. The obtained solids were calcined in a muffle furnace at 150 °C for 4 h.

The Fe_3O_4@g-C_3N_4 composite was dispersed in dimethyl sulfoxide (DMSO) at 0.5 mg·mL^{-1} and ultrasonicated for 15 min to obtain a Fe_3O_4@g-C_3N_4 suspension, which was loaded onto the ceramic membrane at 1 mg·cm^{-2} by vacuum filtration of the as-prepared Fe_3O_4@g-C_3N_4 suspension through the pristine ceramic membrane with an effective membrane area of approximately 17.34 cm^2. The membrane was then rinsed by sequential filtering of 50 mL of ethanol, 50 mL of 1:1 DI water/ethanol, and 100 mL of DI water to remove the residual DMSO, followed by desiccation at 70 °C for 60 min.

2.2. Membrane Surface Aging and Characterization. Membrane aging experiments were performed by continuously filtering the 100 mM NaCl solution at 350 L·m^{-2}·h^{-1} under pressure of 1.0 bar (14.5 psi) for 5 days (120 h) through the modified membranes that were applied at an anodic potential of approximately 10 V (corresponding to a current density of 20 mA·cm^{-2}). To analyze membrane aging, cyclic voltammetry (CV) was conducted to measure the electroactive properties of the anode membrane materials before and after applications of DC currents and liquid permeate filtration. Briefly, the standard three-electrode system was established with the two anode membranes as working electrode, the Ag/AgCl (in 1.0 M KCl) as reference electrode, and a 3 mm platinum wire as the counter electrode. CV curves will be mapped on a CHI 700E electrochemical workstation (CH Instrument, USA). All the measured electrochemical potentials are referenced to the Ag/AgCl electrode potential (considered as 0 V). The electrolyte solution is 10 mM $K_3Fe(CN)_6$ (a redox mediator) in 0.5 M KCl as a supporting electrolyte. The CV curves were obtained by sweeping from −0.4 to 1 V versus Ag/AgCl at a scan rate of 0.05 V·s^{-1}. Chronoamperometry (CA) was also conducted in 100 mM NaCl electrolyte at 10 V versus Ag/AgCl. All electrochemical measurements (CV, CA, and EIS) of the ERMs were performed using Ag/AgCl (in 1.0 M KCl) as reference electrode, and a 3 mm platinum wire as the counter electrode.

Electrochemical impedance spectrometry (EIS) was further conducted to investigate the electrochemical properties of the anode membranes. The anode membranes were charged under open circuit potential (OCP) of 0.3 V vs Ag/AgCl at the frequency range of 100 kHz to 0.01 Hz in aqueous solution containing 10 mM $K_3Fe(CN)_6$ with 0.5 M KCl solution. Furthermore, the obtained EIS data were split/fitted into electrolyte resistance, charge-transfer resistance, and resistance of solid/electrolyte interface to examine the changes in electrode conductivity in detail. During EIS measurements, total impedance of the membrane system (Z_m) is measured as a function of frequency (f), and the resulting data are represented on a Nyquist plot. The obtained data are interpreted by using ZSim 3.0 software.

2.3. Electrochemical Membrane Filtration Assessment. Electrochemical membrane filtration experiments were conducted by a dead-end membrane filtration cell as illustrated in Figure S1 in the Supporting Information (SI). Reactive oxygen species (ROSs), reactive chlorine species generation, and bromate generation highly depend on the concentrations of chloride or bromide and applied anode potentials. Thus, the feed solution was prepared with the NaCl or NaBr concentrations of 50 mM, 100 mM, 200 mM, and 400 mM. These high concentrations were selected to facilitate the detection of the byproducts during electrochemical experiments. Moreover, the high salinity conditions are relevant for the brine wastewater generated from oil and natural gas production, which may contain chloride and bromide at a wide range (e.g., 1−200 g·L^{-1}).[37] The applied cell voltage was applied within 3−15 V, resulting in the current density of 1, 5, 10, and 20 mA·cm^{-2} (corresponding to an anodic potential of approximately 1, 2, 5, and 10 V vs Ag/AgCl, respectively). During the electrochemical membrane filtration, the current densities were controlled at fixed levels by a DC power generator (DC power supply YH-302D). The solution pH value can affect the formation of byproducts and was adjusted to 2.0, 7.0, and 13.0, to compare the changes of byproduct formation. The pH value of the feed solution was adjusted with 1.0 M NaOH solution and 1.0 M HCl solution. Filtration lasted for about 1 h. After stabilizing the electrochemical filtration for 15 min, the filtered solution was collected for sample testing every 10 min. The overall porosity (P_r) of the membrane was determined by a gravimetric method. In addition, the membrane mean pore radius (r_m) was determined by the Guerout−Elford−Ferry equation. The permeate flux was calculated by the Darcy's equation and expressed in units of liters per m^2 of membrane per hour (L·m^{-2}·h^{-1}, LMH). The detailed descriptions are provided in section S2, where we compared the changes of permeate flux, membrane porosity, pore size, and surface hydrophobicity before and after the aging experiments as Table S1 and Table S2. Chloride, chlorite, chlorate, bromide, and bromate concentrations in the permeate were measured by a Dionex ICS-1500 ion chromatography system (ICS-1500) equipped with the AS50 autosampler, and an IonPac AS22 column coupled to a conductivity detector (31 mA). For separation of those anions, we used 23 mM NaOH as the eluent. Operation was isothermic at 30 °C with a flow rate of 1 mL·min^{-1}. More details can be found in Supporting Information (section S6).

3. RESULTS AND DISCUSSIONS

3.1. Morphological Characterization before and after Aging Treatment. Figure S2 shows the typical SEM figures of the p-MWCNTs, o-MWCNTs, Fe_3O_4 NPs, g-C_3N_4 sheet, and Fe_3O_4@g-C_3N_4. The MWCNTs diameter and length distributions are 20−40 nm and 5−15 μm as measured from Figure S2a. The pure Fe_3O_4 NPs exhibited a spherical morphology with a size diameter in the range of 200−300 nm (Figure S2c). Figure S 2d shows that the pure g-C_3N_4 sample was composed of different sizes of crystal stacking layers. Figure S2e shows the conjugated state of Fe_3O_4@g-C_3N_4, where g-C_3N_4 is expected to be those irregular

https://doi.org/10.1021/acs.iecr.2c02847
Ind. Eng. Chem. Res. 2022, 61, 14260−14271

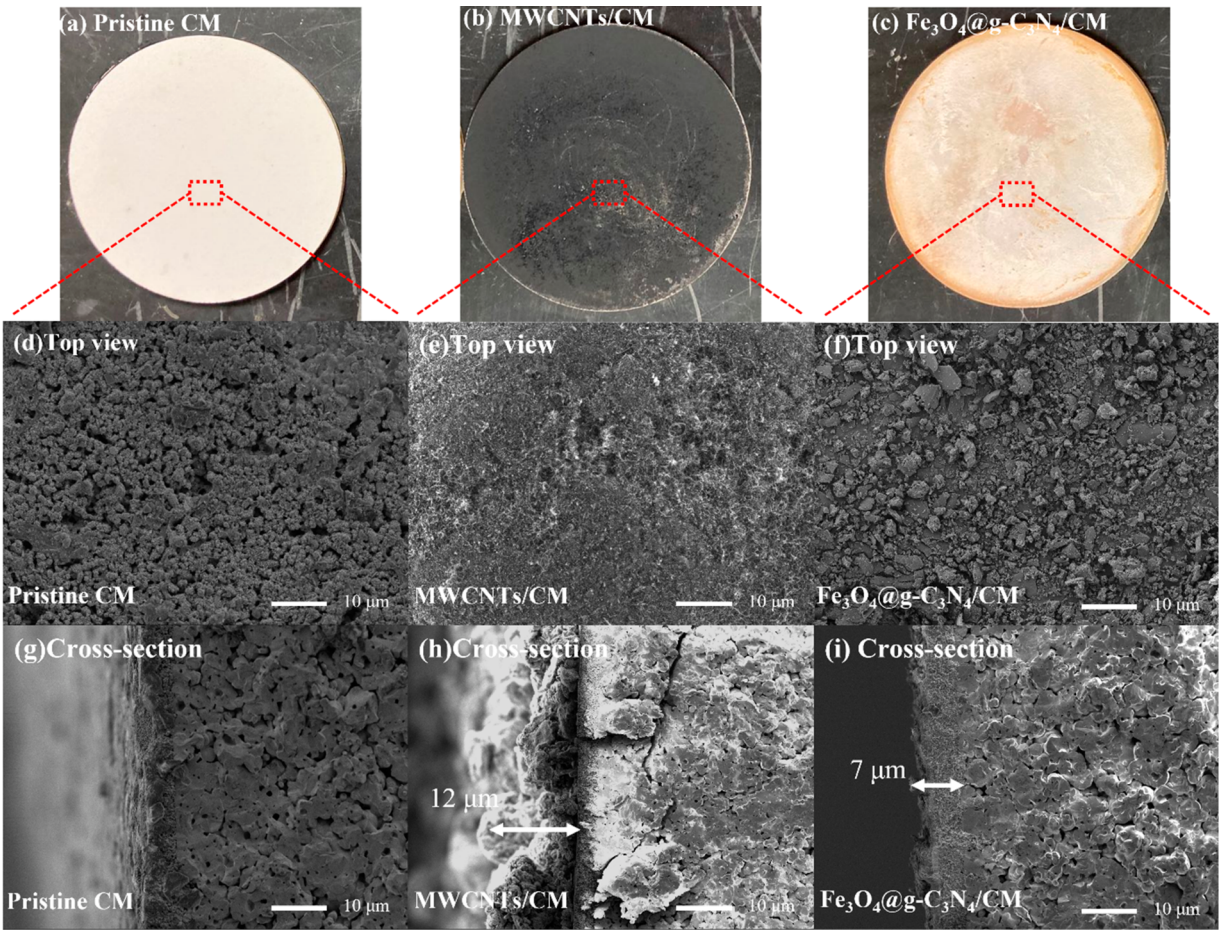

Figure 1. (a–c) Photographs and (d–f) SEM images top view of the pristine CM, MWCNTs/CM, and Fe_3O_4@g-C_3N_4/CM, and (g–i) cross-section of the pristine CM, MWCNTs/CM, and Fe_3O_4@g-C_3N_4/CM.

aggregated particles about several micrometers in size. Moreover, g-C_3N_4 has small pores due to the gas discharge from the melamine decomposition. Fe_3O_4@g-C_3N_4 exhibited a sheet-like structure with spherical Fe_3O_4 NPs deposited on the g-C_3N_4 sheet surfaces as marked in red circles.

The top view and cross-section images of pristine CM, MWCNTs/CM, and Fe_3O_4@g-C_3N_4/CM in Figure 1d and 1f show that the surface of pristine ceramic membranes contains pores with about hundreds of nanometers in diameter, which is consistent with the reported 140 nm pore size by the manufacturer. Figure 1e shows that the coating layer of MWCNTs/CM are in possession of the typical morphology of MWCNTs as shown in Figure S2 and Figure 2b. The cross section images of the MWCNTs/CM indicate that MWCNTs formed a layer with a thickness of ~11 μm. For the Fe_3O_4@g-C_3N_4/CM, Figure 1f shows the ceramic membrane is covered with many irregularly shaped particles. The cross section image of the Fe_3O_4@g-C_3N_4/CM reveals that the layer thickness is ~7 μm.

Figure S3 compares the surface morphology of the two functionalized membranes before and after aging treatment. There are no apparent visual differences for MWCNTs/CM, indicating that the aging treatment had no considerable impacts on the physical integrity of hybridized MWCNTs or its coating structure. Electrochemical oxidation of MWCNTs by the BDD anode was previously reported under 710–2840 mA·cm^{-2}.[38] The oxidized MWCNTs have transformed from a highly bundled state to a debundled state. The amorphous carbon tends to get smaller and become isolated after oxidation, which is not observed in our study. In addition, the SEM images in Figure S3 show significant differences in surface morphology between the pristine and the aged Fe_3O_4@g-C_3N_4/CM. After aging, the bulk graphitic carbon nitride seems to be fractured and has an increased surface roughness. The oxidation treatment of g-C_3N_4 results in the formation of spherical nanoparticles,[39] which may explain the increased surface roughness of the aged membrane. This morphological change might be responsible for the formation of the mesoporous graphitic carbon nitride or oxidized g-C_3N_4.[40]

3.2. Surface Chemical Characterization before and after Aging. Figure 2a shows the FTIR spectra of Fe_3O_4 that has one strong absorption at 590 cm^{-1} assigned to the Fe–O stretching vibration.[41] However, this peak declined in Fe_3O_4@g-C_3N_4 samples due to the reduced content of Fe_3O_4 (5%). Both g-C_3N_4 and Fe_3O_4@g-C_3N_4 yielded the absorption at 810, 1100, 1470, and 1630 cm^{-1} attributed to the breathing and stretching vibrations related to C–N and C═N of triazine units of g-C_3N_4, respectively.[42] Compared with the pristine Fe_3O_4@g-C_3N_4, the aged Fe_3O_4@g-C_3N_4 had an evident decrease of the peak intensity at 1100 cm^{-1} that is assigned to the stretching of the C–N bond (Figure 2b), due to the transformation of C–N into C–O during aging treatment.[43] The FTIR spectra of the *p*-MWCNTs and *o*-MWCNTs show a peak at 1670 cm^{-1} that could be associated with the C═O stretch mode of carboxylic groups due to the acid treatment. Additionally, *o*-MWCNTs show four major peaks at 3230,

https://doi.org/10.1021/acs.iecr.2c02847
Ind. Eng. Chem. Res. 2022, 61, 14260–14271

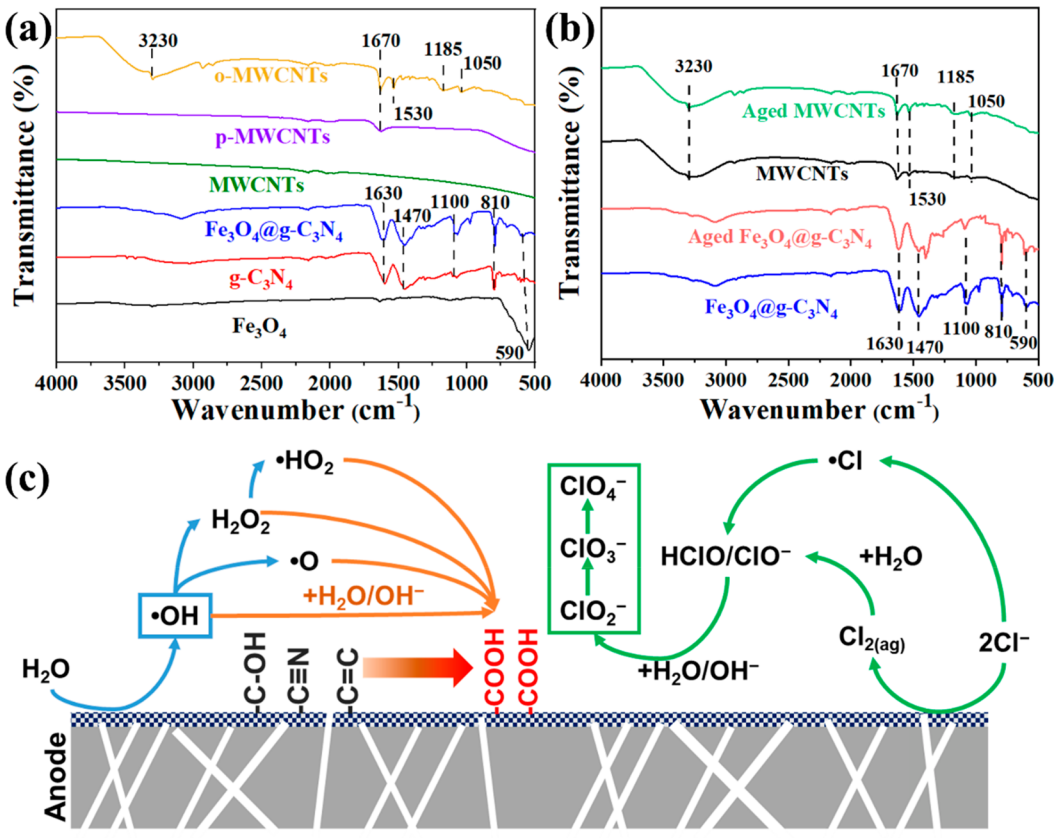

Figure 2. (a) FTIR spectra of Fe_3O_4, g-C_3N_4, Fe_3O_4@ g-C_3N_4, MWCNTs, *p*-MWCNTs and *o*-MWCNTs. (b) FTIR spectra of the pristine Fe_3O_4@ g-C_3N_4, aged Fe_3O_4@ g-C_3N_4, MWCNTs and aged MWCNTs. (c) Proposed mechanism of membrane aging and byproduct formation in filtration process.

1670, 1530, and 1200 cm^{-1}, respectively, which correspond to the hydroxyl groups, the C═C bond stretching, the C═O stretching, and the C−O bond stretching.[44] Moreover, Figure 2b shows that the peak intensities assigned to C═O and C−O bond are slightly higher for the aging membrane when compared to that of the pristine membrane, probably because of the increase of the amount of the new functional groups (e.g., COOH). Li et al. reported two possible mechanisms of interactions between hydroxyl radicals and MWCNTs,[45] radical attack on defect sites and unsaturated bonds of MWCNT sidewalls. XPS results Figure S5 also provide evidence for the aging of two kinds of electrocatalysts as detailed in section S4. For instance, the N−C═N intensity at 396.5 eV for Fe_3O_4@g-C_3N_4 was significantly reduced due to the oxidation of C═N to tertiary nitrogen, secondary amines, and nitroso groups. After aging, the percentage of the carboxyl group peak intensity relative to the total C 1s intensity (13.8%) surpassed that of pristine hybridized MWCNTs (10.7%), implying that electrochemical aging promoted the incorporation of carboxyl groups. This result is supported by a previous study reporting that the carboxyl (−COOH) group could hinder the electrooxidation of pollutants and increase resistance of charge transfer.[46] The aging mechanisms of Fe_3O_4@g-C_3N_4/CM and MWCNTs/CM are depicted in Figure 2c, where C−O, C−N, or C═C are converted to COOH during the aging treatment.

The surface aging of MWCNTs and Fe_3O_4@g-C_3N_4 modified membranes during electrochemical filtration was studied with Raman spectrometry. The top two rows in Figure 3 compare the surface Raman mapping of the pristine and aged MWCNTs/CM membranes. Pristine MWCNTs/CM samples typically exhibit three characteristic Raman peaks at 1344.5, 1581.2, and 2681.2 cm^{-1}, respectively, as shown in Figure S6a, which correspond to the D band, the G band, and the G′ band. The three columns, a, b and c, are images generated based on the intensities of D band, G band, and the ratio of D/G bands, where some regions have higher intensities (red dots) indicative of the presence of MWCNTs. The aged MWCNTs/CM surface had a remarkable reduction in intensity of these Raman signals compared to that of pristine MWCNTs/CM. The ratio between the intensity of D-band and the G-band is slightly higher for an aging membrane when compared to that of the pristine membrane. Moreover, it is possible to identify the locations of the aged MWCNTs on the membrane surface from these mapping images. Similarly, the Raman spectra for the aged Fe_3O_4@g-C_3N_4 in Figure S6b show the G band intensity decreased remarkably similar to the observation on MWCNTs, probably because of the increase of both disordered structures and the amount of the new functional groups (e.g., −COOH) on Fe_3O_4@g-C_3N_4 after the aging process. Accordingly, the I_D/I_G ratios of MWCNTs/CM and Fe_3O_4@g-C_3N_4/CM were found to increase from 20% and 25% to 40% and 50%, respectively, indicating that the two electrocatalyst membranes underwent different aging degrees. The I_D/I_G ratio changes also reflect the transformations of C−O, C═N or C═C groups into COOH groups. The loss of N increased the structural defects (e.g.,

https://doi.org/10.1021/acs.iecr.2c02847
Ind. Eng. Chem. Res. 2022, 61, 14260−14271

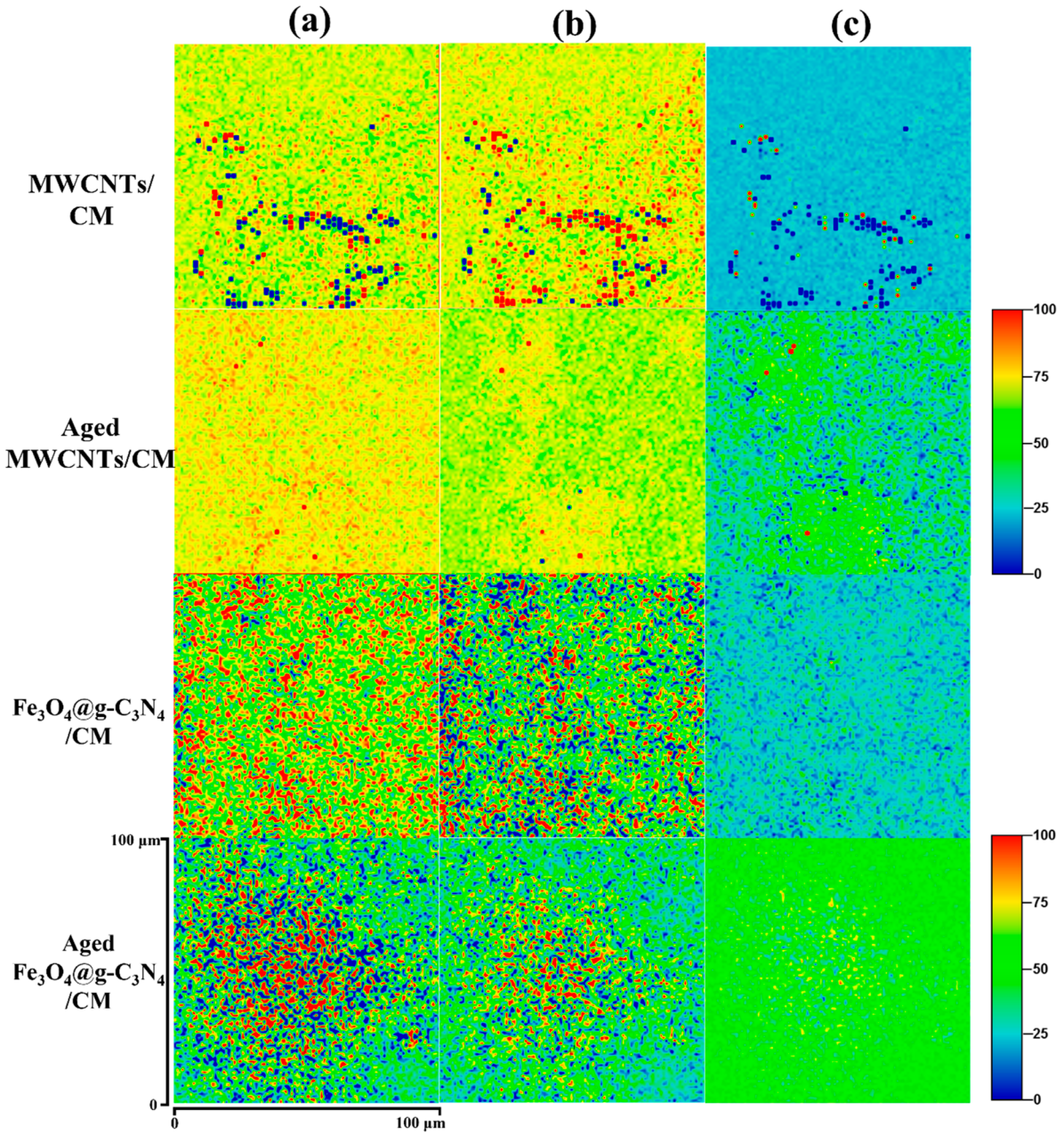

Figure 3. Raman mapping of pristine and aged MWCNTs and Fe_3O_4@g-C_3N_4/CM: (a) D band mapping of the membrane surface, (b) G band mapping of the membrane, (c) I_D/I_G ratio contrast imaging of the membrane surface.

Table 1. Total, Outer and Inner Charge Density, Q_I/Q_T and R_r of the Pristine and Aged MWCNTs and Fe_3O_4 NPs@ g-C_3N_4 Coated Membranes

Membrane	Q_T (mC·cm^{-2})	Q_O (mC·cm^{-2})	Q_I (mC·cm^{-2})	Q_I/Q_T (%)	R_r (unitless)
Pristine MWCNTs/CM	216.91	28.26	188.65	86.97	3615.17
Aged MWCNTs/CM	208.74	26.14	182.60	87.47	3479.00
Pristine Fe_3O_4@g-C_3N_4/CM	140.06	12.06	128.00	91.38	2334.33
Aged Fe_3O_4@g-C_3N_4/CM	130.77	11.11	119.66	91.50	2179.50

nitrogen vacancies) on g-C_3N_4 as indicated by the relatively higher band intensity ratio (I_D/I_G).[47]

3.3. Electrochemical Activity Changes. *3.3.1. Cyclic Voltammetry Assessment for the Pristine and Aged Membranes.* The aging degree is often associated with the reduction of the electrochemically active surface area or electroactive sites. Voltametric charge density (Q) is closely related to the amounts of electroactive sites of a porous electrode and was calculated by integrating the CV curves in Figure S7a–d. Total voltametric charge density (Q_T, mC·cm^{-2}) is the Q value obtained when the scan rate (ν, mV·s^{-1}) is zero as indicated by eq 1 and represents the total electroactive surface charge per surface area.

https://doi.org/10.1021/acs.iecr.2c02847
Ind. Eng. Chem. Res. 2022, 61, 14260−14271

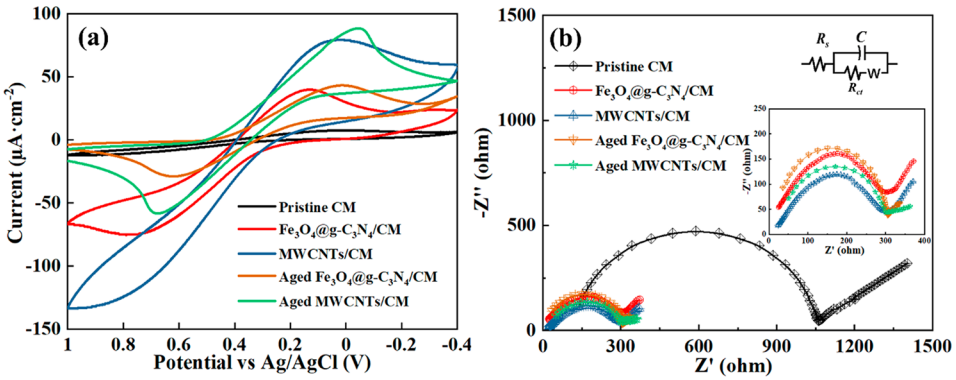

Figure 4. (a) CV curves of the pristine and aged MWCNTs/CM and Fe_3O_4@g-C_3N_4/CM obtained at a sweeping rate of 0.05 V·s^{-1}. (b) EIS spectra of the pristine and aged MWCNTs/CM and Fe_3O_4@g-C_3N_4/CM. (All electrochemical testing use Ag/AgCl (in 1.0 M KCl) as reference electrode, and a 3 mm platinum wire as the counter electrode.)

$$(Q)^{-1} = (Q_T)^{-1} + kv^{1/2} \quad (1)$$

where k is a constant (no unit). Total voltametric charge density (Q_T) is equal to the sum of the outer voltametric charge density (Q_O) and the inner voltametric charge density (Q_I), which represent the charge related to the outer geometric and the inner unattainable electrode areas, respectively. The ratio between Q_I and Q_T (Q_I/Q_T) is equal to the electrochemical porosity. Q_O is related to the easiest attachable electroactive surface area. Q_T and Q_O for the pristine and aged MWCNTs/CM or Fe_3O_4 NPs@ g-C_3N_4/CM samples were determined using eq 1 and 2 with the data in Figure S7 panels e and f, respectively.

$$Q = Q_O + kv^{-1/2} \quad (2)$$

The determined voltametric charges, electrochemical porosity, and roughness factor (R_r) are listed in Table 1, which shows that the outer voltametric charge of the pristine MWCNTs/CM was greater than that of the Fe_3O_4 NPs@ g-C_3N_4/CM. Thus, the MWCNTs/CM yielded a greater number of active sites than Fe_3O_4 NPs@g-C_3N_4/CM. After aging treatment, the outer voltametric charge of the MWCNTs/CM or Fe_3O_4 NPs@g-C_3N_4/CM decreased due to the limited membrane aging. The electrochemical porosity of the MWCNTs/CM or Fe_3O_4 NPs@ g-C_3N_4/CM increase slightly, showing that the aging process exerts a minor influence on the catalytic behavior of the conductive membrane. R_r as an indicator or electrocatalytic activity is the electroactive surface area (ECSA) divided by the geometrical area of the electrode (i.e., R_r = ECSA/geometrical area).[48] The ECSA of membrane electrodes is often calculated using the normalization constant of 60 μC·cm^{-2}. The geometrical area (17.34 cm^2) was then used to calculate the roughness factor. Similar to voltametric charges, R_r of two-membrane electrode decreased after aging, suggesting the loss of catalytic activity of the aged membrane.[49]

Furthermore, Figure 4a compares the CVs of the different membrane samples. Without surface coating, the pristine ceramic membrane yielded negligible peak currents at all the sweep potentials, suggesting low electrochemical activity. By contrast, with the coating of MWCNTs or Fe_3O_4@g-C_3N_4, the typical electrochemical reversible current curves are observed. The peak current of MWCNTs/CM is achieved at 0.04 V and is greater than that of Fe_3O_4@g-C_3N_4 at 0.14 V, which indicates a higher interfacial charge transport on the MWCNTs coating surface. For the aged membrane, the peak currents, especially under the high positive potential bias, decreased significantly for both coated membranes, implying the partial loss of the electrochemical activity or reactive sites on MWCNTs and Fe_3O_4@g-C_3N_4 as mentioned above. To better assess their performance and stability during aging experiments, these two electrochemical membranes were subjected to chronoamperometry at 10 V vs Ag/AgCl. Figure S8 shows that MWCNTs/CM yielded a relatively stable current (~15 mA·cm^{-1}) over time, whereas Fe_3O_4@g-C_3N_4/CM exhibited an initial high current density (~20 mA·cm^{-1}) that progressively declined to 10 mA·cm^{-1} and eventually dropped to 8 mA·cm^{-1} at day 5 due to the oxidative aging. The electrochemical activity of MWCNT/CM generally remained higher than that of Fe_3O_4@g-C_3N_4/CM after the same aging treatment.

3.3.2. Electrochemical Impedance Assessment for the Pristine and Aged Membranes. To analyze the changes of the interfacial charge-transfer resistance before and after aging treatment, electrochemical impedance spectroscopy (EIS) of the brand-new and aged MWCNTs and Fe_3O_4@g-C_3N_4 modified membranes were studied in the same electrolyte solution (10 mM $K_3Fe(CN)_6$ and 0.5 M KCl) at an open circuit potential (0.3 V). The EIS spectra are presented as a Nyquist plot in Figure 4b. The diameter of the semicircle arc of MWCNTs and Fe_3O_4@g-C_3N_4 modified electrodes was significantly smaller than the diameter of the semicircle arc of the pristine membrane, suggesting a faster interfacial charge transport on the coated membrane surface than on the pristine membrane surface.[50] The EIS spectra were fitted with an equivalent circuit as shown in the inset of Figure 4b, where R_{ct} is the charge-transfer resistance at the electrode/solution interface, R_s represents the electrolyte resistance, C is the electrode double-layer capacitance formed at electrode/solution interface. W is the Warburg impedance that models the diffusion process in the dielectric spectroscopy. The value of R_{ct} was further converted to resistivity (R^*_{ct}) using the surface area and coating thickness of the catalyst layer. The results of R_{ct}, R^*_{ct}, R_s, C, and W are summarized in Table 2. Smaller resistances under the MWCNTs composite were obtained compared to that for the Fe_3O_4@g-C_3N_4 composite.

Ceramic membranes made of alumina (Al_2O_3) and zirconia oxides (ZrO_2) also exhibit electrochemical impedance responses as reported previously.[51] Thus, Table 2 demonstrates that the charge transfer resistance (R_{ct}) of the pristine CM reached up to 1000 ohm due to the semiconducting

https://doi.org/10.1021/acs.iecr.2c02847
Ind. Eng. Chem. Res. 2022, 61, 14260−14271

Table 2. Fitted Results of the Parameters in the Equivalent Circuit for Pristine CM and Two Modified CM before and after the Aging Experiments

Electrode	Parameters	Before aging	After aging
Pristine CM	R_s (ohm)	58 ± 10	NA
	R_{ct} (ohm)	1015 ± 105	NA
	C (F)	8.51×10^{-9}	NA
	W ($S \cdot s^{1/2}$)	0.0012	NA
MWCNTs/CM	R_s (ohm)	37.4 ± 3	35.4 ± 5
	R_{ct} (ohm)	220.3 ± 12	248.1 ± 3
	R^*_{ct} (ohm·cm)	3820.1 ± 69.2	4302.2 ± 53.02
	C (F)	3.95×10^{-7}	3.65×10^{-7}
	W ($S \cdot s^{1/2}$)	0.0056	0.0068
Fe_3O_4@g-C_3N_4/CM	R_s (ohm)	43.5 ± 5	44.5 ± 4
	R_{ct} (ohm)	290.2 ± 11	299.6 ± 3
	R^*_{ct} (ohm·cm)	5032.1 ± 90.7	5195.2 ± 98.5
	C (F)	3.68×10^{-7}	3.45×10^{-7}
	W ($S \cdot s^{1/2}$)	0.0067	0.0075

nature of ceramic membranes. The R_{ct} values of MWCNTs (220.3 ± 12) and Fe_3O_4@g-C_3N_4 (290.2 ± 11ohm) modified membranes were significantly smaller than that of the pristine membrane, suggesting a good conductivity on the coated membrane surface and supporting MWCNTs, and the Fe_3O_4@g-C_3N_4 coating converted the pristine CM to a conductive CM. Li et al. also reported that the CNT coating could covert the charge transfer resistance of the Al_2O_3 CM support, around 3000 ohm, to the CNT-coated Al_2O_3 CM of only approximately 200 ohm.[52]

By contrast, the charge transfer resistance (R_{ct}) of two aged electrochemical membranes increased from 220.3 ± 12 ohm to 248.1 ± 3 ohm and from 290.2 ± 11ohm to 299.6 ± 3 ohm, respectively. This increase mainly resulted from the restructuring, irreversible phase transition, and reduction of electroactive sites as described above and elsewhere.[53] For example, the decrease of the electrochemically active surface area results in a reduced electrode double-layer capacitance (C), which agrees with our results in Table 2. Warburg impedance (W) reflects the diffusion process of the electrolyte. Table 2 shows that Warburg impedance increases after aging, implying that the diffusion resistance of the electrolyte within the solid electrode increased. This phenomenon could be caused by the expansion of electrode materials or pore clogging.[54] The electrochemical aging process could have changed the pore size of membranes due to formation of holes, broken layers, partial unzipping, and debundling of MWCNTs,[55] which will hinder efficient diffusion of the redox species from the bulk electrolyte into the pores.[53,56]

3.4. Analysis of Halogenated Byproduct Formation.

3.4.1. Comparison of Halogenated Byproduct Formation on Two Electrochemical Membranes. The generation of chlorine related byproducts during electrochemical membrane filtration is initiated by the oxidation of chloride at the anode surface, which follows the general oxidation pathway as shown in Figure 2c ($Cl^- \rightarrow Cl\cdot \rightarrow HOCl/OCl^- \rightarrow ClO_2^- \rightarrow ClO_3^- \rightarrow ClO_4^-$).[57−59] However, halogen oxides byproduct generation highly depends on the electrode materials.[60] The halogenated byproduct formation on the two presented composite conductive membranes has not been reported elsewhere. Figure 5 shows the halogenated anions such as ClO_2^-, ClO_3^-, and BrO_3^- present in the filtrate from the anodic membrane with the feed solutions made of different concentrations of NaCl or NaBr with two MWCNTs/CM and Fe_3O_4@g-C_3N_4/CM electrodes. Perchlorate was not detected in the filtered water under the current experimental conditions. During electrochemical filtration, Cl^- or Br^- could directly react with the electrode or indirectly with reactive oxygen species (hydroxyl radicals or ozone) to produce oxyanions. Chlorate and bromate formed with a lower level in the Fe_3O_4@g-C_3N_4/CM experiment than that in the MWCNTs/CM experiment. The efficiency of oxidant generation in the electrochemical process depends on the applied anodic potential and adsorption enthalpy of M−OH on electrode materials.[61]

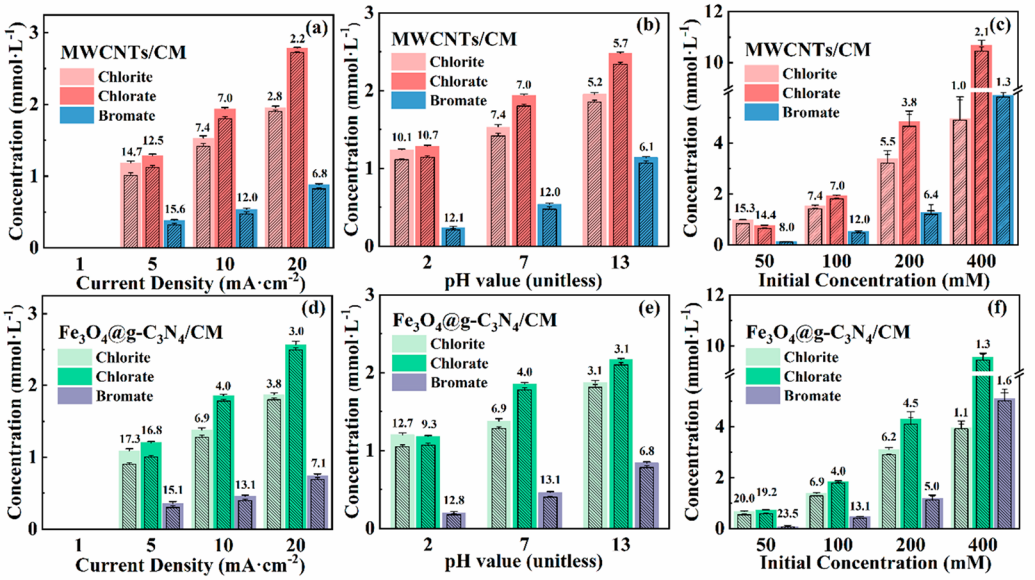

Figure 5. Changes of concentrations of chlorite, chlorate, and bromate of two electrochemical membranes before and after electrochemical aging (a,d) 1−20 mA·cm^{-2} current density with initial concentration 100 mM at pH = 7; (b,e) initial pH = 2−7 with initial concentration 100 mM and current density = 10 mA·cm^{-2}; and (c,f) initial concentration 50−400 mM with current density = 10 mA·cm^{-2} at pH = 7. (The subcolumns with line pattern are concentrations after aging and the labeled numbers stand for the percentage change after electrochemical aging.)

https://doi.org/10.1021/acs.iecr.2c02847
Ind. Eng. Chem. Res. 2022, 61, 14260−14271

During electrolysis, ·OH is produced from water as a surficial intermediate. M−OH denotes ·OH radicals that are physically adsorbed at a surface site. The results suggest that MWCNTs provide more effective catalytic ability and generate more electrogenerated hydroxyl radicals than Fe_3O_4@g-C_3N_4 under the same anodic potentials. Wu et al. confirmed that carbon nanotube electrodes could also produce hydroxyl radicals in electrolysis processes.[62] After the electrochemical aging process, the concentrations of all halogenated anions decreased due to the loss of catalyst activity or reactive sites. After membrane aging, oxygen-containing functional groups were introduced that are capable of interfering with electron transport in the sp2 carbonaceous structure.[63] Fe_3O_4@g-C_3N_4/CM had a relativity higher reduction in halogenated byproduct production than MWCNTs/CM did, due to the relatively lower stability of g-C_3N_4 and Fe_3O_4 than MWCNTs during electrochemical aging as indicated by the XPS results (section S4).[64]

3.4.2. Effect of Current Density on Halogenated Byproduct Formation. Figure 5a shows the effect of the current density on the oxychloride anions distribution. The produced levels of chlorite, chlorate, and bromate increased at high current densities (~20 mA·cm^{-2}), which increase the electron transfer rates and favor hydroxyl radicals' formation. Thus, the rate of chloride oxidation to chlorite or chlorate increased. More importantly, high current densities yield high anodic potentials, which is essential for activating the anodic oxidation reactions of these halogen anions as listed in eqs S5−S9. For instance, the Visual MINTEQ simulation indicates that hypochlorous acid (HOCl) and hypochlorite ions (OCl^-) will be involved when the oxidation/reduction potential is higher than 1 V as shown in Figure S9. Even after the electrochemical aging process, the concentrations of halogenated anions under a high current density only did not change significantly. By contrast, at low current densities (<5 mA·cm^{-2}), there was almost no chlorite, chlorate, or bromate production. The electrochemical aging would significantly cause reduction (above 10%) of the chlorinated or brominated byproducts under low current density. However, lowering current densities or anodic potentials could reduce the oxidation efficacy of water micropollutants. For example, anodic potentials of 3−14 V were needed to mineralize 1,4-dioxane on TiO_2 and Ti/IrO_2−Ta_2O_5.[65,66] PFASs require even higher anodic potentials (e.g., 4−15 V on Ti/RuO_2[67,68]) for oxidative degradation. Thus, when treating these recalcitrant micropollutants in saline water, there could be sizable amounts of halogen oxyanions produced.

3.4.3. Effect of pH on Halogenated Byproduct Formation. The summarized major reactions in eqs S5−S9 clearly indicate the involvement of protons in many reactions, and thus the solution pH could sensitively affect the formation of oxyanions and their speciation. Our results in Figure 5b compare the electrochemical byproducts of oxychloride/bromide anions in acidic (pH = 2), neutral (pH = 7), and basic (pH = 13) conditions using 100 mM NaCl or NaBr solutions under a current density of 10 mA cm^{-2}. The formation of ClO_2^- and ClO_3^- increased with an increase in the initial pH values of the solution and remained constant at higher pH conditions. This result is due to the fact that, at acidic pH (pH = 2), the dominant chlorine species is hypochlorous acid, and the electrochemical oxidation of HOCl (eq S5) would contribute less to the formation of ClO_3^- than does the OCl^- (eq S6). If the solution pH is neutral or alkaline, HOCl is likely converted into of ClO_2^- and ClO_3^-, which agrees with experimental observations. The MINTEQ simulations in Figure S9 confirm that the HOCl concentration decreased as a function of pH increase. At acidic pH values, gaseous chlorine could be promoted, reducing available anionic oxychloride species for oxidation reactions and formation of halogenated oxyanions. Thus, for the aged MWCNTs/CM and Fe_3O_4@g-C_3N_4/CM, reducing the solution pH could greatly inhibit the byproduct formation.

3.4.4. Effect of the Initial Concentration of Salts. Increasing the initial concentration of Cl^- and Br^- generally increases the reaction kinetics of electrochemical oxidation. Figure 5c shows the formation of ClO_2^-, ClO_3^-, and BrO_3^- during the electrochemical filtration of the solutions with varied initial NaCl or NaBr concentrations (50, 100, 200, and 400 mM). The concentrations of chlorite, chlorate, or bromate all increased appreciably with an increase in the Cl^- or Br^- concentrations, which matches the result reported previously.[69] After electrochemical aging, the percentage change of chlorate concentrations are 19.2, 4.0, 4.5, and 1.3% for the initial Cl^- concentrations of 50, 100, 200, and 400 mM under MWCNTs/CM, respectively. The electrochemical aging process will not affect the chlorinated or brominated byproducts formation when the initial Cl^- concentrations is high. The amount of ClO_2^- could not be precisely measured because the produced ClO_2^- could rapidly react with other oxidants, such as O_3 and ·OH, or directly react on the anode to form stable ClO_3^-. Less ClO_4^- could be generated with a higher initial Cl^- content (50−250 mg·L^{-1}) due to the limitation in reactive sites on the electrode.[70] The reactive sites on the electrode will be occupied by excessive Cl^- and then inhibit the ClO_3^- to form ClO_4^-.

4. CONCLUSION

Electrochemical membrane filtration has proven effective for pollutant degradation or chemical conversion in water/wastewater treatment and resource recovery. The high surface area, microporous structures, and tunable reactivity of electrochemically reactive membranes garner the enhanced reaction efficiency and pollutant removal. However, the membrane properties could change with time due to membrane fouling or aging. Particularly, the aging mechanisms for electrochemical membranes remain largely elusive, due to the lack of in-depth research and analysis. Most prior studies only employed limited testing time (1−5 h) to evaluate the conductive membrane filters (e.g., CNT[22] and β-PbO_2[71]) or employed electrolytes that have different water chemistries from reality.[24] The presented electrochemical assessment (CV and EIS) combined with electron microscope imaging, FTIR, XPS, and Raman spectrometry reveals a comprehensive picture of the interfacial chemical state changes and electrochemical activity reduction of MWCNTs and Fe_3O_4@g-C_3N_4 membranes after filtering high-salinity water under high currents (~20 mA·cm^{-2}) and long-term operation (5 days). This aging assessment is essential to fully understand the membrane aging risks and determine operational limits of the applied currents or potentials for the development of novel electrode filters or membranes. The results lay groundwork to guide the practical and scalable applications of ERM filtration for water/wastewater treatment.

The utilization of electrochemical membrane filtration as decentralized point-of-use and point-of-entry water/wastewater treatment seems to be promising. However, the

https://doi.org/10.1021/acs.iecr.2c02847
Ind. Eng. Chem. Res. 2022, 61, 14260−14271

formation of potentially toxic or carcinogenic organic and inorganic byproducts on electrified filtration must be carefully addressed. The natural water may contain chloride (10−100 ppm) and bromide (1−2 ppm), which leads to potential formation of ClO_3^-, ClO_4^-, or BrO_3^- via electrochemical oxidation. Our study examined the chlorite, chlorate, and bromate byproducts formation under different current densities on different anode materials, different initial solution pHs, and different salt concentrations. Clearly, proper adjustment of the operational strategies, including lowering the anodic oxidization potential and lowering the feed solution pH values, may reduce the likelihood of ClO_3^- or BrO_3^- formation. The use of electrochemical membranes for water/wastewater treatment applications will require optimization of operating conditions and possibly a multibarrier approach.

■ ASSOCIATED CONTENT

Supporting Information

The Supporting Information is available free of charge at https://pubs.acs.org/doi/10.1021/acs.iecr.2c02847.

Experiment setup, SEM characterization of membrane, cyclic voltammetry under different scan rate, MINTEQ simulations, and QA/QC (PDF)

■ AUTHOR INFORMATION

Corresponding Author

Wen Zhang − *John A. Reif, Jr. Department of Civil and Environmental Engineering, New Jersey Institute of Technology, Newark, NJ 07102, United States;* orcid.org/0000-0001-8413-0598; Phone: +1-976-596-5520; Email: wen.zhang@njit.edu

Authors

Qingquan Ma − *John A. Reif, Jr. Department of Civil and Environmental Engineering, New Jersey Institute of Technology, Newark, NJ 07102, United States*

Jianan Gao − *John A. Reif, Jr. Department of Civil and Environmental Engineering, New Jersey Institute of Technology, Newark, NJ 07102, United States*

Courtney Potts − *Department of Chemistry and Environmental Science, New Jersey Institute of Technology, Newark, NJ 07102, United States*

Xiao Tong − *Center for Functional Nanomaterials, Brookhaven National Laboratory, Upton, NY 11973, United States*

Yi Tao − *Guangdong Provincial Engineering Research Center for Urban Water Recycling and Environmental Safety, Tsinghua Shenzhen International Graduate School, Tsinghua University, Shenzhen 518055, P.R. China*

Complete contact information is available at: https://pubs.acs.org/10.1021/acs.iecr.2c02847

Notes

The authors declare no competing financial interest.

■ ACKNOWLEDGMENTS

The authors gratefully acknowledge funding support from the New Jersey Water Resources Research Institute (NJWRRI) Grant (Project Number: 2020NJ025B), NSF PFI grant (Award number: 2016472), NSF INTERN grant (Award number: 1836036), National Natural Science Foundation of China (52070117), and the United States Environmental Protection Agency (US EPA) P3 Program under Assistance Agreement No. (83945201). The NSF and the EPA have not formally reviewed this study. The views expressed in this document are solely those of authors and do not necessarily reflect those of the agencies. The NSF and EPA do not endorse any products or commercial services mentioned in this publication. This research used resources of the Center for Functional Nanomaterials (CFN), which is a U.S. Department of Energy Office of Science User Facility, at Brookhaven National Laboratory. The authors also thank the technical consultation and support from BRISEA Inc. High school intern Saachi Kuthari from Millburn High School contributed to the literature review.

■ REFERENCES

(1) Lin, H.; Peng, H.; Feng, X.; Li, X.; Zhao, J.; Yang, K.; Liao, J.; Cheng, D.; Liu, X.; Lv, S. Energy-efficient for advanced oxidation of bio-treated landfill leachate effluent by reactive electrochemical membranes (REMs): Laboratory and pilot scale studies. *Water Res.* **2021**, *190*, 116790.

(2) Zhang, Z.; Huang, G.; Li, Y.; Chen, X.; Yao, Y.; Ren, S.; Li, M.; Wu, Y.; An, C. Electrically conductive inorganic membranes: A review on principles, characteristics and applications. *Chemical Engineering Journal* **2022**, *427*, 131987.

(3) Xie, J.; Ma, J.; Zhao, S.; Waite, T. D. Flow anodic oxidation: Towards high-efficiency removal of aqueous contaminants by adsorbed hydroxyl radicals at 1.5 V vs SHE. *Water Res.* **2021**, *200*, 117259.

(4) Li, J.; Ma, J.; Dai, R.; Wang, X.; Chen, M.; Waite, T. D.; Wang, Z. Self-Enhanced Decomplexation of Cu-Organic Complexes and Cu Recovery from Wastewaters Using an Electrochemical Membrane Filtration System. *Environ. Sci. Technol.* **2021**, *55*, 655−664.

(5) Chaplin, B. P. The prospect of electrochemical technologies advancing worldwide water treatment. *Acc. Chem. Res.* **2019**, *52*, 596−604.

(6) Liang, S.; Lin, H.; Yan, X.; Huang, Q. Electro-oxidation of tetracycline by a Magneli phase Ti4O7 porous anode: Kinetics, products, and toxicity. *Chemical Engineering Journal* **2018**, *332*, 628−636.

(7) Anis, S. F.; Lalia, B. S.; Lesimple, A.; Hashaikeh, R.; Hilal, N. Electrically conductive membranes for contemporaneous dye rejection and degradation. *Chemical Engineering Journal* **2022**, *428*, 131184.

(8) Rui, J.; Deng, N.; Zhao, Y.; Tao, C.; Zhou, J.; Zhao, Z.; Huang, X. Activation of persulfate via Mn doped Mg/Al layered double hydroxide for effective degradation of organics: Insights from chemical and structural variability of catalyst. *Chemosphere* **2022**, *302*, 134849.

(9) Trellu, C.; Rivallin, M.; Cerneaux, S.; Coetsier, C.; Causserand, C.; Oturan, M. A.; Cretin, M. Integration of sub-stoichiometric titanium oxide reactive electrochemical membrane as anode in the electro-Fenton process. *Chemical Engineering Journal* **2020**, *400*, 125936.

(10) Pan, Z.; Yu, F.; Li, L.; Liu, M.; Song, C.; Yang, J.; Li, H.; Wang, C.; Pan, Y.; Wang, T. Low-cost electrochemical filtration carbon membrane prepared from coal via self-bonding. *Chemical Engineering Journal* **2020**, *385*, 123928.

(11) Hua, L.; Guo, L.; Thakkar, M.; Wei, D.; Agbakpe, M.; Kuang, L.; Magpile, M.; Chaplin, B. P.; Tao, Y.; Shuai, D.; Zhang, X.; Mitra, S.; Zhang, W. Effects of anodic oxidation of a substoichiometric titanium dioxide reactive electrochemical membrane on algal cell destabilization and lipid extraction. *Bioresource technology* **2016**, *203*, 112−117.

(12) Zaky, A. M.; Chaplin, B. P. Mechanism of p-Substituted Phenol Oxidation at a Ti4O7 Reactive Electrochemical Membrane. *Environ. Sci. Technol.* **2014**, *48*, 5857−5867.

(13) Ahmed, F.; Lalia, B. S.; Kochkodan, V.; Hilal, N.; Hashaikeh, R. Electrically conductive polymeric membranes for fouling prevention and detection: A review. *Desalination* **2016**, *391*, 1−15.
(14) Lee, A.; Elam, J. W.; Darling, S. B. Membrane materials for water purification: design, development, and application. *Environmental Science: Water Research & Technology* **2016**, *2*, 17−42.
(15) Dudchenko, A. V.; Rolf, J.; Russell, K.; Duan, W.; Jassby, D. Organic fouling inhibition on electrically conducting carbon nanotube-polyvinyl alcohol composite ultrafiltration membranes. *Journal of membrane science* **2014**, *468*, 1−10.
(16) Duan, W.; Ronen, A.; Walker, S.; Jassby, D. Polyaniline-coated carbon nanotube ultrafiltration membranes: enhanced anodic stability for in situ cleaning and electro-oxidation processes. *ACS Appl. Mater. Interfaces* **2016**, *8*, 22574−22584.
(17) Yin, X.; Li, X.; Hua, Z.; Ren, Y. The growth process of the cake layer and membrane fouling alleviation mechanism in a MBR assisted with the self-generated electric field. *Water research* **2020**, *171*, 115452.
(18) Asif, M. B.; Zhang, Z. Ceramic membrane technology for water and wastewater treatment: A critical review of performance, full-scale applications, membrane fouling and prospects. *Chemical Engineering Journal* **2021**, *418*, 129481.
(19) Pan, Z.; Song, C.; Li, L.; Wang, H.; Pan, Y.; Wang, C.; Li, J.; Wang, T.; Feng, X. Membrane technology coupled with electrochemical advanced oxidation processes for organic wastewater treatment: Recent advances and future prospects. *Chemical Engineering Journal* **2019**, *376*, 120909.
(20) Wang, D.; Saleh, N. B.; Sun, W.; Park, C. M.; Shen, C.; Aich, N.; Peijnenburg, W. J.; Zhang, W.; Jin, Y.; Su, C. Next-generation multifunctional carbon-metal nanohybrids for energy and environmental applications. *Environ. Sci. Technol.* **2019**, *53*, 7265−7287.
(21) Zhang, T. Y.; Shao, Y. Y.; Chen, J.; Fan, H. B. In *Study and preparation of electrocatalytic ceramic membrane electrode*; Advanced Materials Research, Trans Tech Publ: 2011; pp 30−35.
(22) Wang, X.; Sun, M.; Zhao, Y.; Wang, C.; Ma, W.; Wong, M. S.; Elimelech, M. In situ electrochemical generation of reactive chlorine species for efficient ultrafiltration membrane self-cleaning. *Environ. Sci. Technol.* **2020**, *54*, 6997−7007.
(23) Zhao, Y.; Deng, N.; Fan, Z.; Hu, Z.-T.; Fan, L.; Zhou, J.; Huang, X. On-site H2O2 electro-generation process combined with ultraviolet: A promising approach for odorous compounds purification in drinking water system. *Chemical Engineering Journal* **2022**, *430*, 132829.
(24) Garcia-Segura, S.; Qu, X.; Alvarez, P. J.; Chaplin, B. P.; Chen, W.; Crittenden, J. C.; Feng, Y.; Gao, G.; He, Z.; Hou, C.-H. Opportunities for nanotechnology to enhance electrochemical treatment of pollutants in potable water and industrial wastewater-a perspective. *Environmental Science: Nano* **2020**, *7*, 2178−2194.
(25) Halali, M. A.; Larocque, M.; de Lannoy, C.-F. Investigating the stability of electrically conductive membranes. *J. Membr. Sci.* **2021**, *627*, 119181.
(26) Halali, M. A.; de Lannoy, C.-F. Methods for stability assessment of electrically conductive membranes. *MethodsX* **2022**, *9*, 101627.
(27) Anglada, Á.; Urtiaga, A.; Ortiz, I.; Mantzavinos, D.; Diamadopoulos, E. Boron-doped diamond anodic treatment of landfill leachate: evaluation of operating variables and formation of oxidation by-products. *Water research* **2011**, *45*, 828−838.
(28) Yang, Y.; Hoffmann, M. R. Synthesis and stabilization of blue-black TiO2 nanotube arrays for electrochemical oxidant generation and wastewater treatment. *Environ. Sci. Technol.* **2016**, *50*, 11888−11894.
(29) Zhang, C.; He, D.; Ma, J.; Waite, T. D. Active chlorine mediated ammonia oxidation revisited: Reaction mechanism, kinetic modelling and implications. *Water research* **2018**, *145*, 220−230.
(30) Li, X.; Huang, G.; Chen, X.; Huang, J.; Li, M.; Yin, J.; Liang, Y.; Yao, Y.; Li, Y. A review on graphitic carbon nitride (g-C3N4) based hybrid membranes for water and wastewater treatment. *Science of The Total Environment* **2021**, *792*, 148462.
(31) Zhang, Y.; Chen, Z.; Zhou, L.; Wu, P.; Zhao, Y.; Lai, Y.; Wang, F.; Li, S. Efficient electrochemical degradation of tetrabromobisphenol A using MnO2/MWCNT composites modified Ni foam as cathode: Kinetic analysis, mechanism and degradation pathway. *Journal of hazardous materials* **2019**, *369*, 770−779.
(32) Pourzamani, H.; Mengelizadeh, N.; Hajizadeh, Y.; Mohammadi, H. Electrochemical degradation of diclofenac using three-dimensional electrode reactor with multi-walled carbon nanotubes. *Environmental Science and Pollution Research* **2018**, *25*, 24746−24763.
(33) Wu, Y.; Chen, M.; Yan, X.; Ren, J.; Dai, Y.; Wang, J.; Pan, J.; Wang, Y.; Cheng, X. Hydrothermal synthesis of Fe3O4 nanorods/graphitic C3N4 composite with enhanced supercapacitive performance. *Mater. Lett.* **2017**, *198*, 114−117.
(34) Song, Q.; Yang, C.; Yu, C.-M. The green one-step electrodeposition of oxygen-functionalized porous gC 3 N 4 decorated with Fe 3 O 4 nanoparticles onto Ni-foam as a binder-free outstanding material for supercapacitors. *New J. Chem.* **2021**, *45*, 657−670.
(35) Liang, S.; Li, G.; Tian, R. Multi-walled carbon nanotubes functionalized with a ultrahigh fraction of carboxyl and hydroxyl groups by ultrasound-assisted oxidation. *J. Mater. Sci.* **2016**, *51*, 3513−3524.
(36) Kumar, S.; T, S.; Kumar, B.; Baruah, A.; Shanker, V. Synthesis of magnetically separable and recyclable g-C3N4-Fe3O4 hybrid nanocomposites with enhanced photocatalytic performance under visible-light irradiation. *J. Phys. Chem. C* **2013**, *117*, 26135−26143.
(37) Sun, M.; Lowry, G. V.; Gregory, K. B. Selective oxidation of bromide in wastewater brines from hydraulic fracturing. *water research* **2013**, *47*, 3723−3731.
(38) Reipa, V.; Hanna, S. K.; Urbas, A.; Sander, L.; Elliott, J.; Conny, J.; Petersen, E. J. Efficient electrochemical degradation of multiwall carbon nanotubes. *Journal of hazardous materials* **2018**, *354*, 275−282.
(39) Giannakoudakis, D. A.; Seredych, M.; Rodríguez-Castellón, E.; Bandosz, T. J. Mesoporous Graphitic Carbon Nitride-Based Nanospheres as Visible-Light Active Chemical Warfare Agents Decontaminant. *ChemNanoMat* **2016**, *2*, 268−272.
(40) Giannakoudakis, D. A.; Travlou, N. A.; Secor, J.; Bandosz, T. J. Oxidized g-C3N4 nanospheres as catalytically photoactive linkers in MOF/g-C3N4 composite of hierarchical pore structure. *Small* **2017**, *13*, 1601758.
(41) Jabir, M. S.; Nayef, U. M.; Kadhim, W. K. A. Polyethylene glycol-functionalized magnetic (Fe3O4) nanoparticles: A novel DNA-mediated antibacterial agent. *Nano Biomedicine & Engineering* **2019**, *11*, 18−27.
(42) Zhao, Y.; Yu, D.; Zhou, H.; Tian, Y.; Yanagisawa, O. Turbostratic carbon nitride prepared by pyrolysis of melamine. *J. Mater. Sci.* **2005**, *40*, 2645−2647.
(43) Gao, Y.; Zhu, Y.; Lyu, L.; Zeng, Q.; Xing, X.; Hu, C. Electronic structure modulation of graphitic carbon nitride by oxygen doping for enhanced catalytic degradation of organic pollutants through peroxymonosulfate activation. *Environ. Sci. Technol.* **2018**, *52*, 14371−14380.
(44) Zhao, X.; Cheng, L.; Jia, N.; Wang, R.; Liu, L.; Gao, C. Polyphenol-metal manipulated nanohybridization of CNT membranes with FeOOH nanorods for high-flux, antifouling and self-cleaning oil/water separation. *J. Membr. Sci.* **2020**, *600*, 117857.
(45) Rong-Ming, L. W. C.; Yi-Wei, X. X.-C. C.; Ming-Li, S., Effect of Hydroxyl Radical on the Surface and Structure of Multi-walled Carbon Nanotubes [J]. *Chinese Journal of Inorganic Chemistry* **2005**, *2*.
(46) Gao, G.; Pan, M.; Vecitis, C. D. Effect of the oxidation approach on carbon nanotube surface functional groups and electrooxidative filtration performance. *Journal of Materials Chemistry A* **2015**, *3*, 7575−7582.
(47) Liao, Y.; Wang, G.; Wang, J.; Wang, K.; Yan, S.; Su, Y. Nitrogen vacancy induced in situ g-C3N4 pn homojunction for boosting visible light-driven hydrogen evolution. *J. Colloid Interface Sci.* **2021**, *587*, 110−120.

(48) Sukeri, A.; Saravia, L. P. H.; Bertotti, M. A facile electrochemical approach to fabricate a nanoporous gold film electrode and its electrocatalytic activity towards dissolved oxygen reduction. *Phys. Chem. Chem. Phys.* **2015**, *17*, 28510−28514.
(49) Alekseeva, O. K.; Mikhalev, A. I.; Lutikova, E. K.; Porembsky, V. I.; Presnyakov, M. Y.; Fateev, V. N.; Shapir, B. L.; Grigoriev, S. A. Structural and electrocatalytic properties of platinum and platinum-carbon layers obtained by magnetron-ion sputtering. *Catalysts* **2018**, *8*, 665.
(50) Li, X.; Li, H.; Li, M.; Li, C.; Sun, D.; Lei, Y.; Yang, B. Preparation of a porous boron-doped diamond/Ta electrode for the electrocatalytic degradation of organic pollutants. *Carbon* **2018**, *129*, 543−551.
(51) Tsui, E. M.; Cortalezzi, M. M.; Wiesner, M. R. Proton conductivity and methanol rejection by ceramic membranes derived from ferroxane and alumoxane precursors. *J. Membr. Sci.* **2007**, *306*, 8−15.
(52) Li, P.; Yang, C.; Sun, F.; Li, X.-y. Fabrication of conductive ceramic membranes for electrically assisted fouling control during membrane filtration for wastewater treatment. *Chemosphere* **2021**, *280*, 130794.
(53) Friedl, J.; Stimming, U. Determining electron transfer kinetics at porous electrodes. *Electrochim. Acta* **2017**, *227*, 235−245.
(54) Kleiner, K.; Melke, J.; Merz, M.; Jakes, P.; Nagel, P.; Schuppler, S.; Liebau, V.; Ehrenberg, H. Unraveling the degradation process of LiNi0. 8Co0. 15Al0. 05O2 electrodes in commercial lithium ion batteries by electronic structure investigations. *ACS Appl. Mater. Interfaces* **2015**, *7*, 19589−19600.
(55) Senokos, E.; Rana, M.; Santos, C.; Marcilla, R.; Vilatela, J. J. Controlled electrochemical functionalization of CNT fibers: structure-chemistry relations and application in current collector-free all-solid supercapacitors. *Carbon* **2019**, *142*, 599−609.
(56) Starov, V. M.; Zhdanov, V. G. Effective viscosity and permeability of porous media. *Colloids Surf., A* **2001**, *192*, 363−375.
(57) Cheng, C.; Kelsall, G. Models of hypochlorite production in electrochemical reactors with plate and porous anodes. *J. Appl. Electrochem.* **2007**, *37*, 1203−1217.
(58) Lin, M.-H.; Bulman, D. M.; Remucal, C. K.; Chaplin, B. P. Chlorinated byproduct formation during the electrochemical advanced oxidation process at Magnéli phase Ti4O7 electrodes. *Environ. Sci. Technol.* **2020**, *54*, 12673−12683.
(59) Hubler, D. K.; Baygents, J. C.; Chaplin, B. P.; Farrell, J. Understanding chlorite, chlorate and perchlorate formation when generating hypochlorite using boron doped diamond film electrodes. *ECS Trans.* **2014**, *58*, 21.
(60) Sun, M.; Wang, X.; Winter, L. R.; Zhao, Y.; Ma, W.; Hedtke, T.; Kim, J.-H.; Elimelech, M. Electrified Membranes for Water Treatment Applications. *ACS ES&T Engineering* **2021**, *1*, 725−752.
(61) Jeong, J.; Kim, C.; Yoon, J. The effect of electrode material on the generation of oxidants and microbial inactivation in the electrochemical disinfection processes. *Water Res.* **2009**, *43*, 895−901.
(62) Wu, D.; Lu, G.; Zhang, R.; Lin, Q.; Yan, Z.; Liu, J.; Li, Y. Enhanced hydroxyl radical generation in the combined ozonation and electrolysis process using carbon nanotubes containing gas diffusion cathode. *Environmental Science and Pollution Research* **2015**, *22*, 15812−15820.
(63) Wang, H.; Dai, H. Strongly coupled inorganic-nano-carbon hybrid materials for energy storage. *Chem. Soc. Rev.* **2013**, *42*, 3088−3113.
(64) Shi, M.; Yang, C.; Yan, C.; Jiang, J.; Liu, Y.; Sun, Z.; Shi, W.; Jian, G.; Guo, Z.; Ahn, J.-H. Boosting ion dynamics through superwettable leaf-like film based on porous g-C3N4 nanosheets for ionogel supercapacitors. *NPG Asia Materials* **2019**, *11*, 1−11.
(65) Jasmann, J. R.; Gedalanga, P. B.; Borch, T.; Mahendra, S.; Blotevogel, J. Synergistic Treatment of Mixed 1, 4-Dioxane and Chlorinated Solvent Contaminations by Coupling Electrochemical Oxidation with Aerobic Biodegradation. *Environ. Sci. Technol.* **2017**, *51*, 12619−12629.
(66) Jasmann, J. R.; Borch, T.; Sale, T. C.; Blotevogel, J. Advanced electrochemical oxidation of 1, 4-dioxane via dark catalysis by novel titanium dioxide (TiO2) pellets. *Environ. Sci. Technol.* **2016**, *50*, 8817−8826.
(67) Schaefer, C. E.; Andaya, C.; Urtiaga, A.; McKenzie, E. R.; Higgins, C. P. Electrochemical treatment of perfluorooctanoic acid (PFOA) and perfluorooctane sulfonic acid (PFOS) in groundwater impacted by aqueous film forming foams (AFFFs). *Journal of Hazardous Materials* **2015**, *295*, 170−175.
(68) Gomez-Ruiz, B.; Gómez-Lavín, S.; Diban, N.; Boiteux, V.; Colin, A.; Dauchy, X.; Urtiaga, A. Efficient electrochemical degradation of poly-and perfluoroalkyl substances (PFASs) from the effluents of an industrial wastewater treatment plant. *Chemical Engineering Journal* **2017**, *322*, 196−204.
(69) Bergmann, M. H.; Rollin, J.; Iourtchouk, T. The occurrence of perchlorate during drinking water electrolysis using BDD anodes. *Electrochim. Acta* **2009**, *54*, 2102−2107.
(70) Bergmann, M. H.; Rollin, J. Product and by-product formation in laboratory studies on disinfection electrolysis of water using boron-doped diamond anodes. *Catal. Today* **2007**, *124*, 198−203.
(71) Yang, K.; Xu, J.; Lin, H.; Xie, R.; Wang, K.; Lv, S.; Liao, J.; Liu, X.; Chen, J.; Yang, Z. Developing a low-pressure and super stable electrochemical tubular reactive filter: Outstanding efficiency for wastewater purification. *Electrochim. Acta* **2020**, *335*, 135634.

https://doi.org/10.1021/acs.iecr.2c02847
Ind. Eng. Chem. Res. 2022, 61, 14260−14271